INORGANIC CHEMISTRY FRONTIERS

CCS 中国化学会 CHINESE CHEMICAL SOCIETY

ROYAL SOCIETY OF CHEMISTRY

Peculiarities of crystal structures and photophysical properties of Ga(III)/Ln(III) metallacrowns with a non-planar [12-MC-4] core

Journal:	*Inorganic Chemistry Frontiers*
Manuscript ID	QI-RES-12-2019-001647.R1
Article Type:	Research Article
Date Submitted by the Author:	17-Feb-2020
Complete List of Authors:	Nguyen, Tu; EPFL, Eliseeva, Svetlana; Centre de Biophysique Moléculaire CNRS, Chow, Chun; University of Michigan, Department of Chemistry Kampf, Jeffrey; University of Michigan, Chemistry Petoud, Stephane; CNRS, Centre de Biophysique Moléculaire; University of Pittsburgh, Department of Chemistry Pecoraro, Vincent; University of Michigan, Chemistry

ARTICLE

Peculiarities of crystal structures and photophysical properties of Ga^{III}/Ln^{III} metallacrowns with a non-planar [12-MC-4] core

Received 00th January 20xx,
Accepted 00th January 20xx

DOI: 10.1039/x0xx00000x

Tu N. Nguyen,[‡,a,c] Svetlana V. Eliseeva,*[,‡,b] Chun Y. Chow,[a] Jeff W. Kampf,[a] Stéphane Petoud,*[,b] and Vincent L. Pecoraro*[,a]

A new series of gallium(III)/lanthanide(III) metallacrown (MC) complexes (**Ln-1**) was synthesized by the direct reaction of salicylhydroxamic acid (H_3shi) with Ga^{III} and Ln^{III} nitrates in a CH_3OH/pyridine mixture. X-ray single crystal analysis revealed two types of structures depending on whether the nitrate counterion coordinate or not to the Ln^{III}: $[LnGa_4(shi)_4(H_2shi)_2(py)_4(NO_3)](py)_2$ (Ln = Gd^{III}, Tb^{III}, Dy^{III}, Ho^{III}) and $[LnGa_4(shi)_4(H_2shi)_2(py)_5](NO_3)(py)$ (Ln = Er^{III}, Tm^{III}, Yb^{III}). The representative **Tb-1** and **Yb-1** MCs consist of a Tb/$YbGa_4$ core with four [Ga^{III}-N-O] repeating units forming a non-planar ring that coordinates the central Ln^{III} through the oxygen atoms of the four shi^{3-} groups. Two H_2shi^- groups bridge the Ln^{III} to the Ga^{III} ring ions. The Yb^{III} in **Yb-1** is eight-coordinated while the ligation of the nine-coordinated Tb^{III} in **Tb-1** is completed by one chelating nitrate ion. **Ln-1** complexes in the solid state showed characteristic sharp f-f transitions in the visible (Tb, Dy) and near-infrared (Dy, Ho, Er, Yb) spectral ranges upon excitation into the ligand-centered electronic levels at 350 nm. Observed luminescence lifetimes and absolute quantum yields were collected and discussed. For **Yb-1,** luminescence data were also acquired in CH_3OH and CD_3OH solutions and a more extensive analysis of photophysical properties was performed. This work demonstrates that while obtaining highly luminescent lanthanide(III) MCs via a direct synthesis is feasible, many factors such as molar absorptivities, triplet state energies, non-radiative deactivations through vibronic coupling with overtones of O-H, N-H, and C-H oscillators and crystal packing will strongly contribute to the luminescent properties and should be carefully considered.

Introduction

Photoluminescence is a light-emitting process based on the absorption of photons, which brings a compound to an excited state that emits light when returning to the ground state. Photoluminescence can be obtained from a variety of compounds, for example, proteins,[1] organic molecules and polymers,[2, 3] semiconductor nanocrystals (quantum dots),[4-6] inorganic pigments,[7] transition metal complexes,[8] and lanthanide(III) (Ln^{III}) complexes and nanomaterials.[9-11] The unique properties of Ln^{III} compounds that complement those of other luminophores include their characteristic sharp emission bands the wavelengths of which depends on the nature of the Ln^{III} and are non-sensitive to changes in their environments, long luminescence lifetimes, and strong resistance to photobleaching, which make them highly appealing for a broad variety of applications in materials sciences as well as for bioanalysis and biological imaging.[12-28]

Most of Ln^{III} ions are luminescent and exhibit characteristic emission in the visible and/or near-infrared (NIR) ranges due to their electronic transitions within 4f orbitals. However, because of the forbidden nature of most of f-f transitions, Ln^{III} ions are very weak light absorbers, with molar absorptivities (ε) in solution often smaller than 10 M^{-1} cm^{-1}.[29] Thus, the direct excitation of Ln^{III} ions is rather inefficient. To overcome this limitation, chromophoric organic sensitizing ligands named "antenna" that possess large ε are often employed to synthesize luminescent Ln^{III} complexes.[30] With this strategy, the excitation light can be efficiently absorbed in the system and the resulting energy can be transferred to the accepting levels of Ln^{III}. The subsequent f-f emission occurs when the system relaxes back to the ground state. The nature of the chromophoric ligands, their molar absorption coefficients, their abilities to protect Ln^{III} ions from non-radiative deactivations and to efficiently sensitize them are main parameters to consider when designing Ln^{III}-containing luminescent compounds.[31-36]

Our group has recently initiated an innovative approach to create highly luminescent Ln^{III} -based probes and materials by utilizing metallacrown complexes.[37-45] Metallacrowns (MCs) are a unique class of inorganic macrocycles that consist of repeating [Metal-N-O] subunits.[46] With structural similarity to crown ethers, MCs are capable of binding a central metal ion through

[a] Department of Chemistry, Willard H. Dow Laboratories, University of Michigan, Ann Arbor, Michigan 48109, USA.*Email: V. L. Pecoraro, vlpec@umich.edu
[b] Centre de Biophysique Moléculaire, CNRS UPR 4301, F-45071 Orléans Cedex 2, France. *Emails: S.V. Eliseeva, svetlana.eliseeva@cnrs-orleans.fr; S. Petoud, stephane.petoud@inserm.fr
[c] Current address: Helen Scientific Research and Technological Development Co., Ltd, Ho Chi Minh City, Vietnam.

†Electronic Supplementary Information (ESI) available: supplementary tables, figures, mass-spectra and X-ray crystallographic parameters, including CIF files (CCDC 1965633-1965634). See DOI: 10.1039/x0xx00000x

‡These authors contributed equally

the hydroximate oxygen atoms. MCs have been extensively explored in the fields of selective ion recognition,[47-53] molecular magnetism[54-62] and magnetorefrigeration,[63] as well as contrast agents for magnetic resonance imaging (MRI).[64-66] In view of the creation of luminescent Ln^{III}-based compounds, the unique MC scaffolds combine a large number of chromophores able to efficiently absorb and sensitize characteristic Ln^{III} emission in the visible and NIR ranges as well as to protect Ln^{III} from the sources of non-radiative deactivations. Several families of highly luminescent MCs exhibiting characteristic Ln^{III} emission have been described, e.g. Ln^{III}/Zn^{II} MCs with an "encapsulated sandwich" structure[38, 67] and Ln^{III}/Ga^{III} MCs with monomeric[39] or dimeric[41] structures assembled using salicylhydroxamic (H_3shi^{3-}) and benzoic (HOBz), or isophthalic (H_2iph) acids, respectively. In this work, we present the syntheses, peculiarities of crystal structures and photophysical properties of a new series of Ga^{III}/Ln^{III} MCs assembled using a direct reaction of the H_3shi ligand with Ga^{III} and Ln^{III} nitrates.

Experimental

All reagents and chemicals were purchased from commercial sources and used without further purification. All reactions were carried under aerobic conditions.

Preparation of Complexes Ln-1

H_3shi (153.1 mg, 1.0 mmol), $Ln(NO_3)_3{\cdot}xH_2O$ (0.25 mmol) (Ln^{III} = Gd^{III}, Tb^{III}, Dy^{III}, Ho^{III}, Er^{III}, Tm^{III}, and Yb^{III}), and $Ga(NO_3)_3{\cdot}xH_2O$ (255.7 mg, 1.0 mmol) were dissolved in 10 mL methanol. Pyridine (2 mL) and acetic acid (0.1 mL) were added and the mixture was stirred for 20 mins. The solution was filtered and kept undisturbed. X-ray quality crystals form after one day.

$[GdGa_4(shi)_4(H_2shi)_2(py)_4(NO_3)] \cdot (py)_2$ (**Gd-1**). Yield: 131 mg (28%). ESI-MS, calc. for $[M]^-$, $C_{42}H_{26}N_6O_{18}GdGa_4$, 1338.8; found, 1337.9. Anal. Calcd for $GdGa_4C_{72}H_{58}N_{13}O_{21}$: C, 46.06; H, 3.11; N, 9.70. Found: C, 46.02; H, 3.07; N, 9.33.

$[TbGa_4(shi)_4(H_2shi)_2(py)_4(NO_3)] \cdot (py)_2$ (**Tb-1**). Yield: 153 mg (33%). ESI-MS, calc. for $[M]^-$, $C_{42}H_{26}N_6O_{18}TbGa_4$, 1340.5; found, 1339.8. Anal. Calcd for $TbGa_4C_{72}H_{58}N_{13}O_{21}$: C, 46.02; H, 3.11; N, 9.69. Found: C, 46.31; H, 3.20; N, 9.64.

$[DyGa_4(shi)_4(H_2shi)_2(py)_4(NO_3)] \cdot (py)_2$ (**Dy-1**). Yield: 151 mg (32%). ESI-MS, calc. for $[M]^-$, $C_{42}H_{26}N_6O_{18}DyGa_4$, 1344.1; found, 1343.9. Anal. Calcd for $DyGa_4C_{72}H_{58}N_{13}O_{21}$: C, 45.93; H, 3.11; N, 9.67. Found: C, 46.22; H, 3.17; N, 9.49.

$[HoGa_4(shi)_4(H_2shi)_2(py)_4(NO_3)] \cdot (py)_2$ (**Ho-1**). Yield: 147 mg (31%). ESI-MS, calc. for $[M]^-$, $C_{42}H_{26}N_6O_{18}HoGa_4$, 1346.5; found, 1346.8. Anal. Calcd for $HoGa_4C_{72}H_{58}N_{13}O_{21}$: C, 45.87; H, 3.10; N, 9.66. Found: C, 46.10; H, 3.13; N, 9.48.

$[ErGa_4(shi)_4(H_2shi)_2(py)_5](NO_3) \cdot (py)$ (**Er-1**). Yield: 127 mg (27%). ESI-MS, calc. for $[M]^-$, $C_{42}H_{26}N_6O_{18}ErGa_4$, 1348.9; found, 1347.9. Anal. Calcd for $ErGa_4C_{72}H_{58}N_{13}O_{21}$: C, 45.82; H, 3.10; N, 9.65. Found: C, 45.68; H, 3.37; N, 9.35.

$[TmGa_4(shi)_4(H_2shi)_2(py)_5](NO_3) \cdot (py)$ (**Tm-1**). Yield: 166 mg (35%). ESI-MS, calc. for $[M]^-$, $C_{42}H_{26}N_6O_{18}TmGa_4$, 1350.5; found, 1350.8. Anal. Calcd for $TmGa_4C_{72}H_{58}N_{13}O_{21}$: C, 45.78; H, 3.09; N, 9.64. Found: C, 45.48; H, 3.35; N, 9.26.

$[YbGa_4(shi)_4(H_2shi)_2(py)_5](NO_3) \cdot (py)$ (**Yb-1**). Yield: 114 mg (24%). ESI-MS, calc. for $[M]^-$, $C_{42}H_{26}N_6O_{18}YbGa_4$, 1354.6; found, 1353.8. Anal. Calcd for $YbGa_4C_{72}H_{58}N_{13}O_{21}$: C, 45.68; H, 3.09; N, 9.62. Found: C, 45.85; H, 3.30; N, 9.31.

X-Ray Crystallography

Single-crystal X-ray crystallographic data for the **Tb-1** and **Yb-1** MCs were collected at 85(2) K on an Rigaku AFC10K Saturn 944+ CCD-based X-ray diffractometer equipped with a Micromax007HF Cu-target microfocus rotating anode (λ = 1.54187 Å), operated at 1200 W power (40 kV, 30 mA). The data were processed with the program CrystalClear 2.0 and corrected for absorption. The structure was solved and refined with the program SHELXTL (version 6.12).[68] All non-hydrogen atoms were refined anisotropically. Hydrogen atoms were placed in their idealized positions. The structure of **Tb-1** contains large solvent accessible voids totalling 939 $Å^3$ and 107 electrons per unit cell. This region has diffuse electron density and could not be modelled with any chemically reasonable moieties. Thus, the SQUEEZE routine of the PLATON suite of programs[69] was applied to remove the diffraction contribution from these solvent molecules. Experimental parameters and crystallographic data for **Tb-1** and **Yb-1** are provided in Table S1. For other **Ln-1** compounds, unit cell parameters were collected and showed in Table S2.

Photophysical Measurements

Luminescence data were collected on samples placed into 2.4 mm i.d. quartz capillaries or quartz Suprasil cells. Emission and excitation spectra were measured on a Horiba-Jobin-Yvon Fluorolog 3 spectrofluorimeter equipped with either a visible photomultiplier tube (PMT) (220-800 nm, R928P; Hamamatsu), a NIR solid-state InGaAs detector cooled to 77 K (800-1600 nm, DSS-IGA020L; ElectroOptical Systems, Inc., USA), or a NIR PMT (950-1650 nm, H10330-75; Hamamatsu). All spectra were corrected for instrumental functions. Luminescence lifetimes were determined under excitation at 355 nm provided by a Nd:YAG laser (YG 980; Quantel), the signals in the visible and the NIR ranges were detected by the R928 or H10330-75 PMTs. The output signals from the detectors were then fed into a 500 MHz bandpass digital oscilloscope (TDS 754C; Tektronix), transferred to a PC and data were processed with the program Origin 8®. Luminescence lifetimes are averages of three or more independent measurements. Quantum yields were determined with a Fluorolog 3 spectrofluorimeter based on the absolute method using an integration sphere (GMP SA). Each sample was measured several times varying the position of samples. Estimated experimental error for the determination of quantum yields is estimated as ~10 %.

ARTICLE

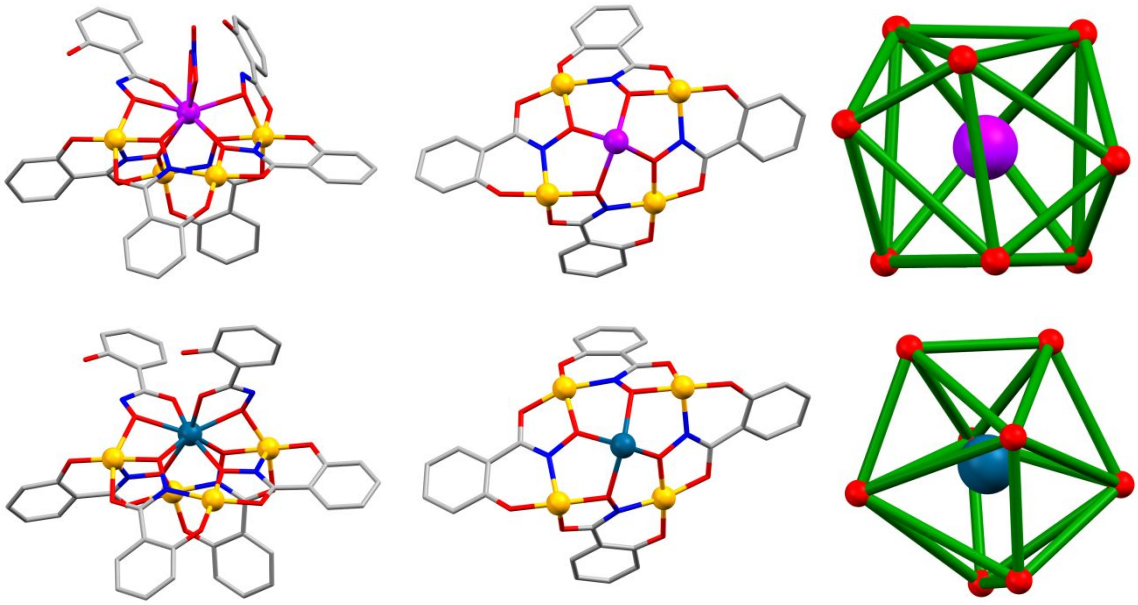

Figure 1 (Top) X-ray crystal structure of **Tb-1** in side-view (left), top-down view of the bent [12-MC-4] core (middle), and coordination geometry around the central Tb^{III} ion (right). (Bottom) X-ray crystal structure of **Yb-1** in side-view (left), top-down view of the bent [12-MC-4] core (middle), and coordination geometry around the central Yb^{III} ion (right). Hydrogen atoms and solvent molecules have been omitted for clarity. Color code: Tb purple; Yb cyan; Ga yellow; O red; N blue; C grey.

Absorption Spectroscopy

Solid-state UV-Vis spectra were collected with the help of an Agilent-Cary 5000 spectrophotometer equipped with a Praying Mantis diffuse reflectance accessory. Spectra were collected in reflectance (*R*) mode. The signal of $BaSO_4$ was used as the reference to establish the baseline. Samples (10 wt. %) were mulled in $BaSO_4$ (90 wt. %). The spectra were then converted into Kubelka-Munk function to represent more accurately the absorption and plotted *vs*. wavelength. UV-Vis absorption spectra of the compounds dissolved in CH_3OH were recorded on a Cary 100Bio UV-Vis spectrophotometer in absorbance mode.

ESI-Mass Spectrometry

ESI-MS spectra were collected with a Micromass LCT time-of-flight electrospray mass spectrometer in a negative ion mode at cone voltages ranging from -40 to -70 V on samples dissolved in CH_3OH. Samples were injected via syringe pump. Data were processed with the program MassLynx 4.0.

Results

Syntheses

The reaction between H_3shi and nitrates of Ga^{III} and Ln^{III} (Gd^{III}, Tb^{III}, Dy^{III}, Ho^{III}, Er^{III}, Tm^{III}, and Yb^{III}) in a CH_3OH/pyridine mixture in presence of a small amount of acetic acid affords **Ln-1** complexes. The general reaction is shown in Scheme 1. The synthetic conditions were similar for all the Ln^{III} salts used in the reactions. The complexes with early Ln^{III} ions such as Nd^{III}, Sm^{III}, and Eu^{III} were formed together with a mixture of unidentified complexes and could not be isolated individually.

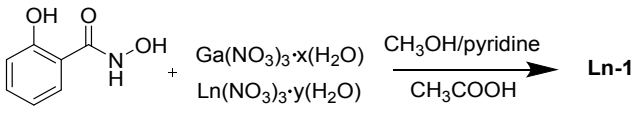

Scheme 1 Synthesis of **Ln-1** complexes.

X-ray crystal structures

Ln-1 complexes crystallize in two different systems as presented in Table S2. The X-ray crystal structures of the two representative molecules, **Tb-1** and **Yb-1,** are shown in Figure 1. Both **Tb-1** and **Yb-1** crystallized in the triclinic $P\bar{1}$ space group. The molecule **Tb-1** contains a $TbGa_4$ core with four [Ga^{III}-N-O] repeating units forming a non-planar [12-MC-4] ring that coordinates the central Tb^{III} ion through the oxygen atoms of the hydroximate groups. The Tb^{III} ion is further bridged to two Ga^{III} ions located in the ring by two mono-deprotonated H_2shi^-

groups and its coordination sphere is filled by a chelating nitrate. The 9-coordinate Tb^{III} ion adopts a coordination geometry close to a tricapped trigonal prism as determined by the program SHAPE (Table S3).[70] **Yb-1** has a similar non-planar [12-MC-4] core as **Tb-1**. The two mono-deprotonated H_2shi^- groups bridge the central Yb^{III} and two Ga^{III} ions located in the ring and result in an eight-coordinated Yb^{III} ion that adopts a coordination geometry close to triangular dodecahedron (Table S4). The charge of the **Yb-1** complex is balanced by one nitrate counter anion**.**

Photophysical properties

Ligand-centered photophysical properties. The UV-Vis absorption spectra of H_3shi and **Ln-1** complexes were collected in CH_3OH solutions. Reflectance spectra of **Ln-1** complexes were collected in the solid state. H_3shi exhibits broad absorption bands in solution resulting from $\pi \rightarrow \pi^*$ transitions in the UV region extending up to 340 nm with an apparent maximum of the band centered at ~300 nm ($\varepsilon = 3.9 \cdot 10^3$ M^{-1} cm^{-1}, Figure 2). **Ln-1** complexes display a slight red shift of their corresponding absorption bands in solution, as shown in Figure 2 for the **Gd-1** complex (Figure S1, top for all **Ln-1** complexes) associated with large molar absorptivities ($\varepsilon_{\mathbf{Gd\text{-}1}} = 3.29 \cdot 10^4$ M^{-1} cm^{-1} at 307 nm) due to the combined contribution of the six ligands derived from H_3shi. Diffuse reflectance spectra of the **Ln-1** complexes (Figure S1, bottom) are dominated by broad bands that correspond to the contribution of the ligands. Sharper bands with significantly lower intensities are observed above wavelength values of 400 nm. These narrow bands can unambiguously be assigned to f-f transitions of the corresponding Ln^{III} ions, and are particularly pronounced for Ho^{III} and Er^{III} ions (Figure S1, bottom). UV-Vis absorption and reflectance spectra of the **Ln-1** complexes are nearly superimposable indicating that the nature of the Ln^{III} ions does not significantly affect the electronic structures of the chromophoric ligands and the corresponding positions of the ligand-centered bands.

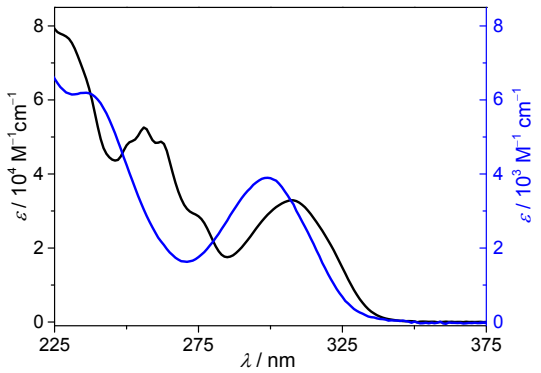

Figure 2 Absorption spectra of the **Gd-1** MC recorded in CH_3OH solutions (black trace, left scale) and H_3shi (blue trace, right scale).

An important factor that is assumed to play a significant role in the sensitization of luminescent Ln^{III} ions in their complexes is the energy position of the triplet state (^3T) of the organic ligands. The energy of the ^3T level in **Ln-1** can be estimated from the phosphorescence spectrum of the corresponding Gd^{III} complex. Phosphorescence intensity is promoted due to heavy-atom and paramagnetic effects induced by the Gd^{III} ion.[71] In addition, the accepting electronic level of Gd^{III} is located at sufficiently high energy (~32 000 cm^{-1})[72] to prevent its population through electronic levels of most organic ligands. **Gd-1** MC exhibits the phosphorescence signal shown in Figure 3. The spectrum was recorded in time-resolved mode in the solid state at 77 K upon excitation at 325 nm and using a 100 µs delay after the excitation flash to remove any fluorescence signal arising from the singlet state. The Gaussian decomposition of the phosphorescence spectrum allowed to estimate the energy of the 0-0 transition, that is located at 461.6 nm (~21 660 cm^{-1}) and represents the energy of the triplet state.

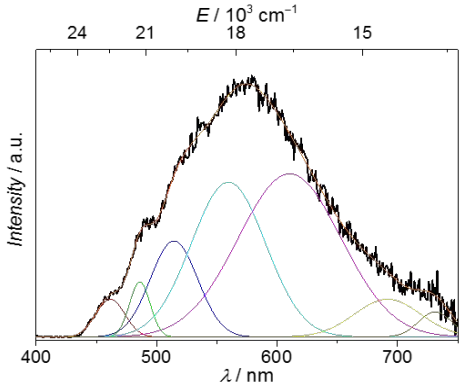

Figure 3 Phosphorescence spectrum of the **Gd-1** MC measured in the solid state under excitation at 325 nm (77 K, 100 µs delay after the excitation flash, black trace) and its Gaussian decomposition (colored traces).

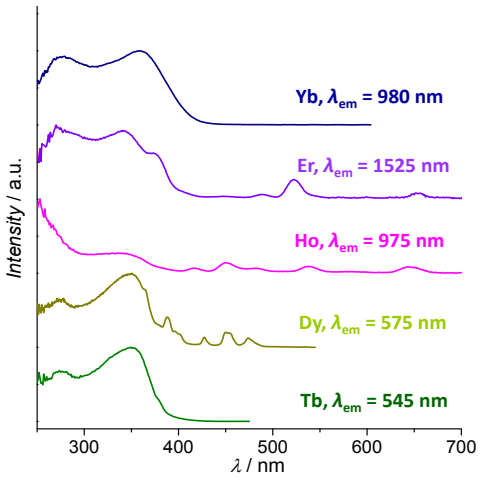

Figure 4 Corrected and normalized excitation spectra of the **Ln-1** MCs in the solid state upon monitoring the main transitions of the corresponding Ln^{III} ions at room temperature.

Lanthanide-centered photophysical properties. Excitation and emission spectra of all **Ln-1** complexes were collected in the solid state. Since Ln^{III} ions exhibit characteristic emission bands, excitation spectra can be obtained by monitoring the specific f-f transitions of the corresponding Ln^{III} ion.

The excitation spectra of the **Ln-1** complexes recorded in the solid state (Figure 4) are similar to the corresponding absorption and reflectance spectra (Figure S1) and exhibit broad bands in the range 250 – 400 nm. This observation indicate that the sensitization of the five Ln^{III} tested here is occurring in each case through the electronic state located on the organic chromophoric part of the MCs. A slight extension towards longer wavelengths is observed due to the saturation effects (Figure S2).[73, 74] In addition, sharper bands with lower intensity that can be attributed to f-f transitions are detected

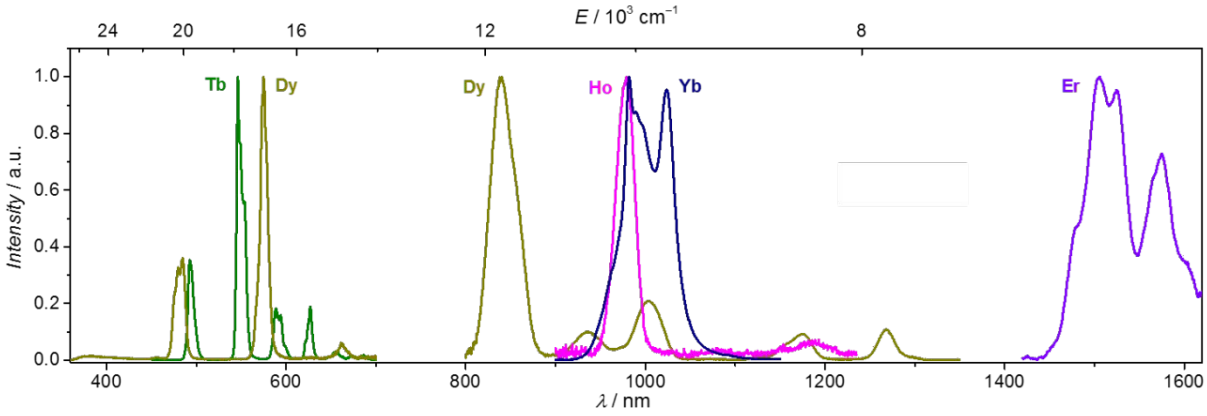

Figure 5 Corrected and normalized emission spectra of the **Ln-1** MCs in the solid state under excitation at 350 nm at room temperature.

for Er^{III}, Ho^{III}, and Dy^{III} MCs. The study of the excitation spectra allows for the determination of the excitation wavelengths of **Ln-1** complexes corresponding to the highest emission intensities, which are ~350 nm for the solid samples. Thus, emission spectra were collected for **Ln-1** samples in the solid state upon excitation at 350 nm at room temperature (Figure 5). Characteristic emissions of Ln^{III} ions in the visible (Tb^{III}), NIR (Ho^{III}, Er^{III}, Yb^{III}) or both (Dy^{III}) regions were observed. Luminescence lifetimes (τ_{obs}) and absolute Ln^{III}-centred quantum yields under ligands excitation (Q^{L}_{Ln}) were also acquired as quantitative luminescence data; the results are summarized in Table 1.

Tb-1 exhibits green emission resulting from the $^5D_4 \rightarrow {}^7F_J$ (J = 6 – 0) transitions. The four prominent bands centered at ~ 493, 545, 589 and 627 nm correspond to $^5D_4 \rightarrow {}^7F_{6,5,4,3}$ transitions whereas the other three transitions $^5D_4 \rightarrow {}^7F_{2,1,0}$ are of significantly lower intensity and observed in the range 640 – 700 nm. The relative integral intensities of different transitions for **Tb-1** are given in Table S2. The solid state sample has ta Q^{L}_{Tb} value of 11.3% and a τ_{obs} of 509 µs.

Dy-1 exhibits a number of bands across the visible and the NIR regions arising from the $^4F_{9/2} \rightarrow {}^6H_J$ (J = 15/2 – 5/2) and $^4F_{9/2} \rightarrow {}^6F_J$ (J = 9/2 – 3/2) electronic transitions. In the visible region, the spectrum is dominated by two bands centered at 483 and 574 nm corresponding to the $^4F_{9/2} \rightarrow {}^6H_{15/2,\ 13/2}$ transitions. These bands are responsible for the apparent yellow-green emission of this MC. In the NIR region, beside the high-intensity band at 840 nm originating from the $^4F_{9/2} \rightarrow {}^6F_{9/2}$, $^6H_{7/2}$ transitions, the emission bands at 937, 1005, 1177 and 1269 nm corresponding to $^4F_{9/2} \rightarrow {}^6H_{5/2,}$ $^4F_{9/2} \rightarrow {}^6F_{7/2}$, $^4F_{9/2} \rightarrow {}^6F_{5/2}$ and $^4F_{9/2} \rightarrow {}^6F_{3/2}$ transitions can be detected. The residual broad ligand-centered emission signal is observed in the 375 – 550 nm range and can be explained by an incomplete energy transfer to Dy^{III} or an energy back transfer from Dy^{III} to the ligands due to the close energy difference between the $^4F_{9/2}$ and the ^3T levels. Measured Dy^{III}-centered quantum yield values of the solid state sample in the visible and the NIR regions are 0.22 and 0.013 %, respectively. The total quantum yield of **Dy-1** in the visible range is 0.23 %, so that the ligand contribution to the total emission can be estimated to 3.9 %.

Ho-1 exhibits a NIR emission of relatively low intensity with maxima at 978 and 1188 nm due to the $^5F_5 \rightarrow {}^5I_7$ and $^5I_6 \rightarrow {}^5I_8$ transitions, respectively. The Q^{L}_{Ho} value of **Ho-1** in the solid state is $1.6 \cdot 10^{-3}$ % and the observed lifetime is equal to 32 ns.

Er-1 exhibits a relatively broad NIR emission band in the range of 1500 – 1620 nm corresponding to the $^4I_{13/2} \rightarrow {}^4I_{15/2}$ transition. The Er^{III}-centered quantum yield is similar to the one of **Ho-1**, $1.55 \cdot 10^{-3}$ %. In contrast, the observed lifetime is significantly longer with a value of 220 ns.

Tm-1 does not exhibit any emission due to f-f transitions or the emission signal is too weak to be detected.

Yb-1 exhibits a NIR emission band in the range 900 – 1150 nm arising from the $^2F_{5/2} \rightarrow {}^2F_{7/2}$ transition. The Q^{L}_{Yb} of the solid state sample is 0.216 %, and the observed luminescence lifetime τ_{obs} is 2.99 µs. Photophysical properties of this sample were also studied in CH_3OH and CD_3OD solutions (Figure 6). It was found that the crystal field splitting of the $^2F_{5/2} \rightarrow {}^2F_{7/2}$ transition is different for the sample in solution compared to the one in the solid state. Such behavior reflects changes in coordination environment around Yb^{III} between the two phases. Indeed, calculations of the hydration number taking into account the values of observed lifetimes collected in CH_3OH and CD_3OD and using the well-established phenomenological equation[75] confirmed the coordination of one solvent molecule to Yb^{III}. The quantum yield value in CD_3OD is 12-fold higher (2.55 %) than

the one obtained in the solid state, however it decreases to 0.12 % in CH_3OH.

Radiative lifetime, intrinsic quantum yield (Q_{Yb}^{Yb}) and sensitization efficiency (η_{sens}) of ***Yb-1***. Radiative lifetime (τ_{rad}) is the lifetime of an electronic state when only radiative processes depopulate this level.

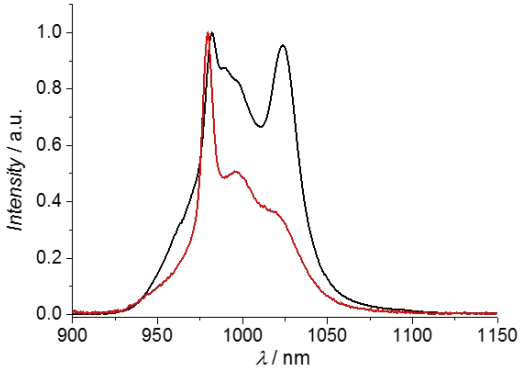

Figure 6 Corrected and normalized emission spectra of the **Yb-1** MC collected in the solid state (λ_{ex} = 350 nm, black trace) and in methanol solutions (λ_{ex} = 320 nm, 0.5 mM, red trace) at room temperature.

In the case of **Yb-1**, τ_{rad} can be calculated from the absorption spectrum in the range of $^2F_{5/2} \leftarrow {}^2F_{7/2}$ transition (Figure 7) using the modified Einstein's equation:[76]

$$\frac{1}{\tau_{rad}} = 2303 \times \frac{8\pi c n^2 \tilde{\nu}_m^2 (2J+1)}{N_A (2J'+1)} \int \varepsilon(\tilde{\nu}) d\tilde{\nu} \quad (1a)$$

$$\tilde{\nu}_m = \frac{\int \tilde{\nu} \varepsilon(\tilde{\nu}) d\tilde{\nu}}{\int \varepsilon(\tilde{\nu}) d\tilde{\nu}} \quad (1b)$$

where c is the speed of light in centimeters per second, n is the refractive index, N_A is the Avogadro's number, J and J' are the quantum numbers for the ground and excited states, respectively, $\int \varepsilon(\tilde{\nu}) d\tilde{\nu}$ is the integrated spectrum of the f-f transition, $\tilde{\nu}_m$ is the barycenter of the transition. It is worth noting that the very low molar absorptivity (< 6 M^{-1} cm^{-1}) is characteristic of free Ln^{III} ions. The obtained value of the radiative lifetime of **Yb-1** is given in Table 2.

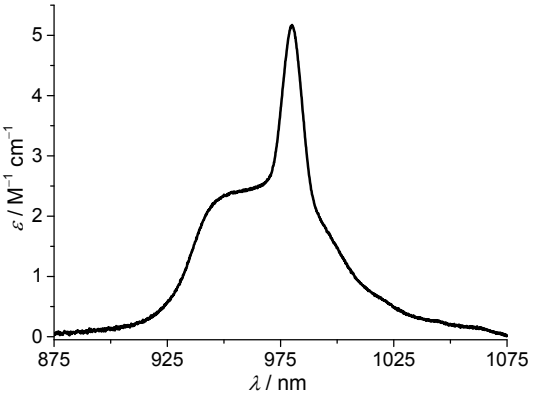

Figure 7 Absorption spectrum of the **Yb-1** MC in the range of $^2F_{5/2} \leftarrow {}^2F_{7/2}$ transition in CH_3OH (1.8 mM) at room temperature.

Having τ_{rad} values in hand together with the values of observed lifetimes and Q_{Yb}^{L}, intrinsic quantum yields (Q_{Yb}^{Yb}) and sensitization efficiencies (η_{sens}) can be calculated using the following equations (2a, 2b):

$$Q_{Yb}^{Yb} = \frac{\tau_{obs}}{\tau_{rad}} \times 100\% \quad (2a)$$

$$\eta_{sens} = \frac{Q_{Yb}^{L}}{Q_{Yb}^{Yb}} \times 100\% \quad (2b)$$

The results are summarized in Table 2 and compared with the values reported previously for $YbGa_4(shi)_4(OBz)_4$[39] and $YbZn_{16}(quinHA)_{16}$[38] MCs.

Discussion

Syntheses

This work focuses on expanding the available luminescent structure types for Ga^{III}shi metallacrowns and seeks to rationalize the photophysics associated with different Ln^{III} environments in this family of molecules. The direct synthesis of MCs is often not straightforward. Therefore, in this work, the reactions between H_3shi and Ga^{III} and a series of Ln^{III} salts were screened under a variety of experimental conditions: solvent, stoichiometry, presence or absence of simple carboxylic acids, *etc*. Reactions of $Ga(NO_3)_3 \cdot xH_2O$, $Ln(NO_3)_3 \cdot yH_2O$ and H_3shi in a 4:1:4 molar ratio in CH_3OH/pyridine led to the isolation of **Ln-1** MCs. The 4:1:4 ratio implies that the Ga^{III} and Ln^{III} salts are in slight excess but the increase of the amount of H_3shi did not improve the yield further. The addition of a small amount of acetic acid was found to be crucial to obtain high quality single crystals of **Ln-1** MCs. The reactions also showed differences in behavior between the early and late Ln^{III} ions. With the same synthetic conditions described in the experimental section, the early Ln^{III} ions (Nd^{III}, Sm^{III}, Eu^{III}) did not form pure **Ln-1** products. The ions located in the middle of the series (Gd^{III}, Tb^{III}, Dy^{III}, Ho^{III}) form complexes in which the Ln^{III} is nine-coordinated. For the complexes formed with the smallest Ln^{III} of the series (Er^{III}, Tm^{III}, Yb^{III}), the Ln^{III} are eight-coordinated.

Table 1 Photophysical data for **Ln-1** complexes at room temperature.[a]

Complex	ΔE (cm^{-1})[b]	τ_{obs} (μs)[c]	Q_{Ln}^{L}(%)[d]
Tb-1	1 260	509(7)	11.3(5)
Dy-1	560	3.36(6)	0.222(6)[e]
Ho-1	6 160	0.032(1)	$1.6(1)\cdot10^{-3}$
Er-1	14 960	0.220(3)	$1.55(3)\cdot10^{-3}$
Yb-1	11 360	2.99(2)	0.216(6)

[a] 2σ values are given between parentheses. Relative errors: τ_{obs}, ±2%; Q_{Ln}^{L}, ±10%. [b] $\Delta E(^3T - E^{Ln})$ is the energy gap between the ligand triplet state (^3T = 21 660 cm^{-1}) and Ln^{III} emissive states: $E^{Tb}(^5D_4)$ = 20 400 cm^{-1}, $E^{Dy}(^4F_{9/2})$ = 21 100 cm^{-1}, $E^{Ho}(^5F_5)$ = 15 500 cm^{-1}, $E^{Er}(^4I_{13/2})$ = 6 700 cm^{-1}, $E^{Yb}(^2F_{5/2})$ = 10 300 cm^{-1}.[77-79] [c] λ_{ex} = 355 nm. [d] λ_{ex} = 350 nm. [e] Total quantum yield including ligand-centered emission is equal to 0.231(8) %.

Table 2 Photophysical properties of the **Yb-1** MC in solution and comparison with other Yb^{III} MCs.[a]

Complex	Solvent	τ_{obs} (μs)	τ_{rad} (ms)[b]	Q_{Yb}^{Yb} (%)	Q_{Yb}^{L} (%)	η_{sens} (%)
Yb-1	CD_3OD	27.4(1)	0.59	4.6	2.55(5)	55
	CH_3OH	1.72(1)	0.59	0.29	0.123(2)	42
$YbGa_4$[c]	CD_3OD	36.6(1)	0.53	6.9	4.29(1)	62
	CH_3OH	2.06(4)	0.53	0.39	0.26(1)	67
$YbZn_{16}$[d]	CD_3OD	150.7(2)	0.68	22.2	2.88(2)	13
	CH_3OH	14.88(1)	0.68	2.2	0.25(1)	11

[a] Relative errors: τ_{obs}, ±2%; Q_{Yb}^{L}, ±10%; τ_{rad}, ±10%; Q_{Yb}^{Yb}, ±12%; η_{sens}, ±22%. [b] Calculated using eq. 1 according to ref. [76]. For CD_3OD solutions, τ_{rad} was recalculated taking into account the difference in refractive indexes, $n(CD_3OD)$ = 1.326.[c] $YbGa_4(shi)_4(OBz)_4$, From ref. [39]. [d] $YbZn_{16}(quinHA)_{16}$, From ref. [38].

Luminescent properties

Ln-1 complexes formed with Tb^{III}, Dy^{III}, Ho^{III}, Er^{III}, and Yb^{III} in the solid state exhibit characteristic emissions arising from f-f transitions in the visible and/or the NIR ranges upon excitation into ligand-centered levels at 350 nm (Figure 5). In the emission spectrum of the **Dy-1** MC, in addition to the Dy^{III}-centered sharp transitions, the residual broad-band ligands emission is observed reflecting an incomplete $^3T \rightarrow {}^4F_{9/2}$ chromophore to Dy^{III} energy transfer and/or the existence of a back $^4F_{9/2} \leftarrow {}^3T$ energy transfer. Indeed, if long-lived triplet states are considered to be the main feeding levels for Ln^{III} ions, the back energy transfer may occur when the ^3T state is too close to the energy of the emitting level of the Ln^{III} ion (E^{Ln}). It is assumed that, when the energy difference $\Delta E(^3T–E^{Ln})$ is < 2000 cm^{-1},[29] there is a high possibility of back energy transfer processes. In the case of **Dy-1**, this energy difference $\Delta E(^3T–{}^4F_{9/2})$ is only 560 cm^{-1}, therefore back energy transfer is highly probable for this MC. The same is true for **Tb-1** with $\Delta E(^3T–{}^4D_4)$ equal to 1260 cm^{-1}. For **Ln-1** MCs formed with all other Ln^{III}, ΔE is > 6000 cm^{-1}, thus preventing a back energy transfer to the ^3T level. It should be noted that the position of the triplet state in **Ln-1** (21 660 cm^{-1}) is very close in energy to those reported previously for the monomeric $LnGa_4(shi)_4(OBz)_4$ (^3T = 22 170 cm^{-1})[39] and for the dimeric $Ln_2Ga_8(shi)_8(iph)_4$ (^3T = 21 980 cm^{-1})[41] MCs assembled using salicylhydroxamic acid. Nevertheless, Ln^{III}-centered quantum yield values collected under ligands excitation (Q_{Ln}^{L}) and observed lifetimes (τ_{obs}) (Table 1) of **Ln-1** MCs are lower than these recorded for $LnGa_4(shi)_4(OBz)_4$[39] or $Ln_2Ga_8(shi)_8(iph)_4$.[28] In the case of **Tb-1** and **Dy-1**, such behavior could be explained by the enhanced back energy transfer processes, while for **Ln-1** MCs formed with other Ln^{III}, the reason most probably lies in the structural feature of **Ln-1** as explained below. In general, Ln^{III}-centered quantum yield values collected under ligands excitation (Q_{Ln}^{L}) and observed luminescence lifetimes (τ_{obs}) (Table 1) of **Ln-1** MCs are following the energy gap law, i.e. the smaller the energy gap between the lowest level of the emitting and the highest level of the ground states, the higher is the probability of the quenching of Ln^{III} through overtones of high energy vibrations, like O–H, N–H, C–H.[80] The highest Q_{Ln}^{L} and the longest τ_{obs} values are observed for **Tb-1** MC, while lower values were measured for **Dy-1**, **Yb-1** and **Er-1**. Ho^{III} ions coordinated in complexes with organic ligands usually exhibit very weak luminescence intensities.[81-84] Nevertheless, for the **Ho-1** MC, quantitative parameters could be accurately acquired (Table 1).

If one considers the environment around the Ln^{III} ions in **Ln-1**, the presence of two incompletely deprotonated H_2shi^- ligands implies N–H and O–H groups being in close proximity to the Ln^{III}. These high-energy oscillators are the main sources of non-radiative deactivations, in particular for Ln^{III} with small energy gaps between the emitting and the ground levels.[29, 31] Such feature of **Ln-1** MCs could explain their lower Q_{Ln}^{L} and shorter τ_{obs} values compared to the previously reported Ln^{III}/Ga^{III} MCs.[39, 41] Moreover, the presence of water and methanol solvent molecules in the lattice of **Ln-1** and intermolecular interactions due to π-π stacking (d = 3.55 Å for **Yb-1**, Figure S3) could serve as additional sources of non-radiative deactivations of Ln^{III} ions and induces the lowering of their luminescence.

To quantitatively assess the parameters that affect Q_{Ln}^{L}, sensitization efficiencies and intrinsic quantum yields have to be estimated. Q_{Ln}^{Ln} can be obtained by the direct excitation of Ln^{III} into f-f transitions; however, such measurements are often tricky due to the low molar absorptivities of f-f transitions. Another method to obtain Q_{Ln}^{Ln} involves the determination of τ_{obs} and τ_{rad} according to eq. 2a. Observed luminescence lifetime can be routinely measured whereas the determination of τ_{rad} is not as straightforward. It is worth noting here that τ_{rad} is specific for the Ln^{III} coordination environment and the electronic transition involved in the emission.[85] This parameter is getting an increased attention recently as controlling τ_{rad} has been shown to be a promising strategy to significantly improve efficiencies of visible- and NIR-emitting Ln^{III} complexes.[86-88] Radiative lifetime can be estimated from the modified Einstein's equation (eq. 1) if the absorption spectrum that corresponds to the emission one is known. Among all studied **Ln-1**, such procedure could be applied only for **Yb-1** in methanol solution. The value of τ_{rad} equal to 0.59 ms was found (Table 2). This parameter is very close to the τ_{rad} value reported for $YbGa_4(shi)_4(OBz)_4$ (0.53 ms)[39] and slightly shorter than the one for $YbZn_{16}(quinHA)_{16}$.[38] Taking into account τ_{obs} and Q_{Yb}^{L} values in the corresponding solvents, Q_{Yb}^{Yb} were estimated to be 4.6% in CD_3OD and 0.29% in CH_3OH with sensitization efficiencies of 55% and 42%, respectively. In comparison to the previously reported Yb^{III} MCs,[38, 39] **Yb-1** exhibits η_{sens} four times higher than the one for $YbZn_{16}(quinHA)_{16}$ and only slightly lower than the one of $YbGa_4(shi)_4(OBz)_4$. However, the Q_{Yb}^{Yb} value for **Yb-1** is 5-7 times lower than in the case of $YbZn_{16}(quinHA)_{16}$ and 1.5 times lower than for $YbGa_4(shi)_4(OBz)_4$. As a result, **Yb-1** has a Q_{Yb}^{L} value in CD_3OD which is only slightly lower than the one for $YbZn_{16}(quinHA)_{16}$ but 1.7 times smaller than the one for $YbGa_4(shi)_4(OBz)_4$. In respect to luminescence efficiency, defined as $Q_{Yb}^{L} \times \varepsilon$, the lower Q_{Yb}^{L} of **Yb-1** in solution compared to $YbGa_4(shi)_4(OBz)_4$ can be almost fully compensated by the 1.5 times higher molar absorptivity of the former due to the contribution of six ligands instead of four shi^{3-} ligands for the latter.

Conclusions

Via direct synthesis, we have obtained and fully characterized a new series of visible and NIR-emitting $LnGa_4$ MCs (**Ln-1**). We have demonstrated that the crystal structure of **Ln-1** depends on the nature of the Ln^{III}. Factors that affect luminescence intensities such as the energy levels of triplet states, molar absorptivities, non-radiative deactivation through vibronic coupling with overtones of O-H, N-H, and C-H oscillators, and crystal packing have been discussed in details. The presence of two incompletely deprotonated H_2shi^- ligands, crystal lattice water and methanol molecules, as well as intermolecular interactions due to π-π stacking in the **Ln-1**, contribute to the non-radiative deactivation of Ln^{III} ions and induce the lowering of their quantum yield values and the shortening of their luminescence lifetimes. This effect, although, is partially compensated by the 1.5-times higher molar absorptivity of **Ln-1** compared to the previously published monomeric $LnGa_4$ MCs.[39] In conclusion, designing MCs is a fully innovative and versatile approach to create lanthanide(III) complexes with high luminescence intensities. With a broad variety of available chromophoric structures, ligands that can be used to form MCs, there is an unprecedented number of possibilities to construct several families of lanthanide(III)-based luminescent MCs with controlled properties that can be used for a broad range of applications from material sciences to bioanalyses and bioimaging.

Conflicts of interest

There are no conflicts to declare.

Acknowledgements

The research leading to these results have received funding from the European Community's Seventh Framework Program (IRSES Metallacrown - FP7/2007-2013) under grant agreement n° 611488. This research was also supported in part by the National Science Foundation under grant CHE-1361779, La Ligue contre le Cancer and La Région Centre. S.P. acknowledges support from Institut National de la Santé et de la Recherche Médicale (INSERM).

References

1. E. A. Rodriguez, R. E. Campbell, J. Y. Lin, M. Z. Lin, A. Miyawaki, A. E. Palmer, X. K. Shu, J. Zhang and R. Y. Tsien, The growing and glowing toolbox of fluorescent and photoactive proteins, *Trends Biochem. Sci.*, 2017, **42**, 111-129.

2. X.-F. Zhang, J. Zhang and L. Liu, Fluorescence properties of twenty fluorescein derivatives: lifetime, quantum yield, absorption and emission spectra, *J. Fluoresc.*, 2014, **24**, 819-826.

3. J. C. Li and K. Y. Pu, Development of organic semiconducting materials for deep-tissue optical imaging, phototherapy and photoactivation, *Chem. Soc. Rev.*, 2019, **48**, 38-71.

4. L. Martínez Maestro, C. Jacinto, U. Rocha, M. Carmen Iglesias-de la Cruz, F. Sanz-Rodriguez, A. Juarranz, J. García Solé and D. Jaque, Optimum quantum dot size for highly efficient fluorescence bioimaging, *J. Appl. Phys.*, 2012, **111**, 023513.

5. K. J. Mintz, Y. Q. Zhou and R. M. Leblanc, Recent development of carbon quantum dots regarding their optical properties, photoluminescence mechanism, and core structure, *Nanoscale*, 2019, **11**, 4634-4652.

6. N. Pradhan, S. Das Adhikari, A. Nag and D. D. Sarma, Luminescence, plasmonic, and magnetic properties of doped semiconductor nanocrystals, *Angew. Chem. Int. Ed.*, 2017, **56**, 7038-7054.

7. S. Banerjee, C. D. Malliakas, J. I. Jang, J. B. Ketterson and M. G. Kanatzidis, $1/\infty[ZrPSe^{6-}]$: a soluble photoluminescent inorganic polymer and strong second harmonic generation response of its alkali salts, *J. Am. Chem. Soc.*, 2008, **130**, 12270-12272.

8. V. W.-W. Yam and K. M.-C. Wong, Luminescent metal complexes of d^6, d^8 and d^{10} transition metal centres, *Chem. Commun.*, 2011, **47**, 11579-11592.

9. L. Armelao, S. Quici, F. Barigelletti, G. Accorsi, G. Bottaro, M. Cavazzini and E. Tondello, Design of luminescent lanthanide complexes: From molecules to highly efficient photo-emitting materials, *Coord. Chem. Rev.*, 2010, **254**, 487-505.

10. T. N. Nguyen, F. M. Ebrahim and K. C. Stylianou, Photoluminescent, upconversion luminescent and nonlinear optical metal-organic frameworks: From fundamental photophysics to potential applications, *Coord. Chem. Rev.*, 2018, **377**, 259-306.

11. J. T. Xu, A. Gulzar, P. P. Yang, H. T. Bi, D. Yang, S. L. Gai, F. He, J. Lin, B. G. Xing and D. Y. Jin, Recent advances in near-infrared emitting lanthanide-doped nanoconstructs: mechanism, design and application for bioimaging, *Coord. Chem. Rev.*, 2019, **381**, 104-134.

12. L. D. Carlos, R. A. S. Ferreira, V. de Zea Bermudez, B. Julian-Lopez and P. Escribano, Progress on lanthanide-based organic-inorganic hybrid phosphors, *Chem. Soc. Rev.*, 2011, **40**, 536-549.

13. J.-C. G. Bünzli, Lanthanide light for biology and medical diagnosis, *J. Lumin.*, 2016, **170**, 866-878.

14. J.-C. G. Bünzli and A.-S. Chauvin, in *Handbook on the Physics and Chemistry of Rare Earths*, eds. J.-C. G. Bünzli and V. K. Pecharsky, Elsevier Science, B.V., Amsterdam, 2013, vol. 44, Ch. 261, pp. 169-282.

15. H. Dong, S. R. Du, X. Y. Zheng, G. M. Lyu, L. D. Sun, L. D. Li, P. Z. Zhang, C. Zhang and C. H. Yan, Lanthanide nanoparticles: from design toward bioimaging and therapy, *Chem. Rev.*, 2015, **115**, 10725-10815.

16. K. Binnemans, Lanthanide-based luminescent hybrid materials, *Chem. Rev.*, 2009, **109**, 4283-4374.

17. J. Feng and H. J. Zhang, Hybrid materials based on lanthanide organic complexes: a review, *Chem. Soc. Rev.*, 2013, **42**, 387-410.

18. M. Sy, A. Nonat, N. Hildebrandt and L. J. Charbonniere, Lanthanide-based luminescence biolabelling, *Chem. Commun.*, 2016, **52**, 5080-5095.

19. I. Martinić, S. V. Eliseeva and S. Petoud, Near-infrared emitting probes for biological imaging: organic fluorophores, quantum dots, fluorescent proteins, lanthanide(III) complexes and nanomaterials, *J. Lumin.*, 2017, **189**, 19-43.

20. G. X. Bai, M. K. Tsang and J. H. Hao, Luminescent ions in advanced composite materials for multifunctional applications, *Adv. Funct. Mater.*, 2016, **26**, 6330-6350.

21. J.-C. G. Bünzli, Lanthanide luminescence for biomedical analyses and imaging, *Chem. Rev.*, 2010, **110**, 2729-2755.

22. T. N. Nguyen, G. Capano, A. Gładysiak, F. M. Ebrahim, S. V. Eliseeva, A. Chidambaram, B. Valizadeh, S. Petoud, B. Smit and K. C. Stylianou, Lanthanide-based near-infrared emitting metal–organic

frameworks with tunable excitation wavelengths and high quantum yields, *Chem. Commun.*, 2018, **54**, 6816-6819.
23. F. M. Ebrahim, T. N. Nguyen, S. Shyshkanov, A. Gładysiak, P. Favre, A. Zacharia, G. Itskos, P. J. Dyson and K. C. Stylianou, Selective, fast-response, and regenerable metal–organic framework for sampling excess fluoride levels in drinking water, *J. Am. Chem. Soc.*, 2019, **141**, 3052-3058.
24. Y. Hasegawa and Y. Kitagawa, Thermo-sensitive luminescence of lanthanide complexes, clusters, coordination polymers and metal-organic frameworks with organic photosensitizers, *J. Mater. Chem. C*, 2019, **7**, 7494-7511.
25. Y. Y. Ning, M. L. Zhu and J. L. Zhang, Near-infrared (NIR) lanthanide molecular probes for bioimaging and biosensing, *Coord. Chem. Rev.*, 2019, **399**.
26. K. Staszak, K. Wieszczycka, V. Marturano and B. Tylkowski, Lanthanides complexes - chiral sensing of biomolecules, *Coord. Chem. Rev.*, 2019, **397**, 76-90.
27. L. D. Wang, Z. F. Zhao, C. Wei, H. B. Wei, Z. W. Liu, Z. Q. Bian and C. H. Huang, Review on the electroluminescence study of lanthanide complexes, *Adv. Opt. Mater.*, 2019, **7**, Art. 1801256.
28. C. D. S. Brites, S. Balabhadra and L. D. Carlos, Lanthanide-based thermometers: at the cutting-edge of luminescence thermometry, *Adv. Opt. Mater.*, 2019, **7**, Art. 1801239.
29. J.-C. G. Bünzli and S. V. Eliseeva, in *Comprehensive Inorganic Chemistry II*, ed. V. W.-W. Yam, Elsevier B.V., Amsterdam, 2013, vol. 8, ch. 8.08, pp. 339-398.
30. H. Uh and S. Petoud, Novel antennae for the sensitization of near infrared luminescent lanthanide cations, *C. R. Chim*, 2010, **13**, 668-680.
31. J.-C. G. Bünzli, On the design of highly luminescent lanthanide complexes, *Coord. Chem. Rev.*, 2015, **293-294**, 19-47.
32. D. Mara, F. Artizzu, P. F. Smet, A. M. Kaczmarek, K. Van Hecke and R. Van Deun, Vibrational quenching in near-infrared emitting lanthanide complexes: a quantitative experimental study and novel insights, *Chem. Eur. J.*, 2019, **25**, 15944-15956.
33. J.-X. Zhang, W.-L. Chan, C. Xie, Y. Zhou, H.-F. Chau, P. Maity, G. T. Harrison, A. Amassian, O. F. Mohammed, P. A. Tanner, W.-K. Wong and K.-L. Wong, Impressive near-infrared brightness and singlet oxygen generation from strategic lanthanide–porphyrin double-decker complexes in aqueous solution, *Light Sci. Appl.*, 2019, **8**, Art. 46.
34. D. Davis, A. J. Carrod, Z. Guo, B. M. Kariuki, Y.-Z. Zhang and Z. Pikramenou, Imidodiphosphonate ligands for enhanced sensitization and shielding of visible and near-infrared lanthanides, *Inorg. Chem.*, 2019, **58**, 13268-13275.
35. S.-Y. Wu, X.-Q. Guo, L.-P. Zhou and Q.-F. Sun, Fine-tuned visible and near-infrared luminescence on self-assembled lanthanide-organic tetrahedral cages with triazole-based chelates, *Inorg. Chem.*, 2019, **58**, 7091-7098.
36. C. Kruck, P. Nazari, C. Dee, B. S. Richards, A. Turshatov and M. Seitz, Efficient ytterbium near-infrared luminophore based on a nondeuterated ligand, *Inorg. Chem.*, 2019, **58**, 6959-6965.
37. J. Jankolovits, C. M. Andolina, J. W. Kampf, K. N. Raymond and V. L. Pecoraro, Assembly of near-infrared luminescent lanthanide host(host-guest) complexes with a metallacrown sandwich motif, *Angew. Chem. Int. Ed.*, 2011, **50**, 9660-9664.
38. E. R. Trivedi, S. V. Eliseeva, J. Jankolovits, M. M. Olmstead, S. Petoud and V. L. Pecoraro, Highly emitting near-infrared lanthanide "encapsulated sandwich" metallacrown complexes with excitation shifted toward lower energy, *J. Am. Chem. Soc.*, 2014, **136**, 1526-1534.
39. C. Y. Chow, S. V. Eliseeva, E. R. Trivedi, T. N. Nguyen, J. W. Kampf, S. Petoud and V. L. Pecoraro, Ga^{3+}/Ln^{3+} metallacrowns: a promising family of highly luminescent lanthanide complexes that covers visible and near-infrared domains, *J. Am. Chem. Soc.*, 2016, **138**, 5100-5109.
40. J. C. Lutter, S. V. Eliseeva, J. W. Kampf, S. Petoud and V. L. Pecoraro, A unique Ln(III){[3.3.1]Ga(III) metallacryptate} series that possesses properties of slow magnetic relaxation and visible/near-infrared luminescence, *Chem. Eur. J.*, 2018, **24**, 10773-10783.
41. T. N. Nguyen, C. Y. Chow, S. V. Eliseeva, E. R. Trivedi, J. W. Kampf, I. Martinić, S. Petoud and V. L. Pecoraro, One-step assembly of visible and near-infrared emitting metallacrown dimers using a bifunctional linker, *Chem. Eur. J.*, 2018, **5**, 1031-1035.
42. I. Martinić, S. V. Eliseeva, T. N. Nguyen, F. Foucher, D. Gosset, F. Westall, V. L. Pecoraro and S. Petoud, Near-infrared luminescent metallacrowns for combined in vitro cell fixation and counter staining, *Chem. Sci.*, 2017, **8**, 6042-6050.
43. I. Martinić, S. V. Eliseeva, T. N. Nguyen, V. L. Pecoraro and S. Petoud, Near-infrared optical imaging of necrotic cells by photostable lanthanide-based metallacrowns, *J. Am. Chem. Soc.*, 2017, **139**, 8388-8391.
44. J. C. Lutter, B. A. Lopez Bermudez, T. N. Nguyen, J. W. Kampf and V. L. Pecoraro, Functionalization of luminescent lanthanide-gallium metallacrowns using copper-catalyzed alkyne-azide cycloaddition and thiol-maleimide Michael addition, *J. Inorg. Biochem.*, 2019, **192**, 119-125.
45. J. C. Lutter, S. V. Eliseeva, G. Collet, I. Martinic, J. W. Kampf, B. L. Schneider, A. Carichner, J. Sobilo, S. Lerondel, S. Petoud and V. L. Pecoraro, Iodinated metallacrowns: toward combined bimodal near-infrared and X-ray contrast imaging agents, *Chem. Eur. J.*, 2020, **26**, 1274-1277.
46. G. Mezei, C. M. Zaleski and V. L. Pecoraro, Structural and functional evolution of metallacrowns, *Chem. Rev.*, 2007, **107**, 4933-5003.
47. A. D. Cutland, R. G. Malkani, J. W. Kampf and V. L. Pecoraro, Lanthanide 15-metallacrown-5 complexes form nitrate-selective chiral cavities, *Angew. Chem. Int. Ed.*, 2000, **39**, 2689-2691.
48. C.-S. Lim, J. Jankolovits, P. Zhao, J. W. Kampf and V. L. Pecoraro, Gd(III) 15-metallacrown-5 recognition of chiral alpha-amino acid analogues, *Inorg. Chem.*, 2011, **50**, 4832-4841.
49. J. T. Grant, J. Jankolovits and V. L. Pecoraro, Enhanced guest affinity and enantioselectivity through variation of the Gd^{3+} 15-metallacrown-5 side chain, *Inorg. Chem.*, 2012, **51**, 8034-8041.
50. C. Sgarlata, A. Giuffrida, E. R. Trivedi, V. L. Pecoraro and G. Arena, Anion encapsulation drives the formation of dimeric Gd(III)[15-metallacrown-5](3+) complexes in aqueous solution, *Inorg. Chem.*, 2017, **56**, 4771-4774.
51. J. Jankolovits, C. S. Lim, G. Mezei, J. W. Kampf and V. L. Pecoraro, Influencing the size and anion selectivity of dimeric Ln^{3+} 15-metallacrown-5 compartments through systematic variation of the host side chains and central metal, *Inorg. Chem.*, 2012, **51**, 4527-4538.
52. J. Jankolovits, A. D. C. Van-Noord, J. W. Kampf and V. L. Pecoraro, Selective anion encapsulation in solid-state Ln(III)[15-metallacrown-5]$^{3+}$ compartments through secondary sphere interactions, *Dalton Trans.*, 2013, **42**, 9803-9808.
53. H. Piotrowski, K. Polborn, G. Hilt and K. Severin, A self-assembled metallomacrocyclic ionophore with high affinity and selectivity for Li^+ and Na^+, *J. Am. Chem. Soc.*, 2001, **123**, 2699-2700.
54. C. Y. Chow, H. Bolvin, V. E. Campbell, R. Guillot, J. W. Kampf, W. Wernsdorfer, F. Gendron, J. Autschbach, V. L. Pecoraro and T. Mallah, Assessing the exchange coupling in binuclear lanthanide(III)

complexes and the slow relaxation of the magnetization in the antiferromagnetically coupled Dy2 derivative, *Chem. Sci.*, 2015, **6**, 4148-4159.

55. T. T. Boron, J. C. Lutter, C. I. Daly, C. Y. Chow, A. H. Davis, A. Nimthong-Roldán, M. Zeller, J. W. Kampf, C. M. Zaleski and V. L. Pecoraro, The nature of the bridging anion controls the single-molecule magnetic properties of dyx4m 12-metallacrown-4 complexes, *Inorg. Chem.*, 2016, **55**, 10597-10607.

56. C. M. Zaleski, S. Tricard, E. C. Depperman, W. Wernsdorfer, T. Mallah, M. L. Kirk and V. L. Pecoraro, Single molecule magnet behavior of a pentanuclear mn-based metallacrown complex: solid state and solution magnetic studies, *Inorg. Chem.*, 2011, **50**, 11348-11352.

57. C. M. Zaleski, E. C. Depperman, J. W. Kampf, M. L. Kirk and V. L. Pecoraro, Using Ln(III)[15-$MC_{Cu(II)(N)(S)\text{-}pheHA}$-5]$^{3+}$ complexes to construct chiral single-molecule magnets and chains of single-molecule magnets, *Inorg. Chem.*, 2006, **45**, 10022-10024.

58. C. M. Zaleski, E. C. Depperman, C. Dendrinou-Samara, M. Alexiou, J. W. Kampf, D. P. Kessissoglou, M. L. Kirk and V. L. Pecoraro, Metallacryptate single-molecule magnets: effect of lower molecular symmetry on blocking temperature, *J. Am. Chem. Soc.*, 2005, **127**, 12862-12872.

59. C. M. Zaleski, E. C. Depperman, J. W. Kampf, M. L. Kirk and V. L. Pecoraro, Synthesis, structure, and magnetic properties of a large lanthanide–transition-metal single-molecule magnet, *Angew. Chem. Int. Ed.*, 2004, **43**, 3912-3914.

60. T. T. Boron, J. W. Kampf and V. L. Pecoraro, A mixed 3d−4f 14-metallacrown-5 complex that displays slow magnetic relaxation through geometric control of magnetoanisotropy, *Inorg. Chem.*, 2010, **49**, 9104-9106.

61. P. Happ and E. Rentschler, Enforcement of a high-spin ground state for the first 3d heterometallic 12-metallacrown-4 complex, *Dalton Trans.*, 2014, **43**, 15308-15312.

62. P. Happ, C. Plenk and E. Rentschler, 12-MC-4 metallacrowns as versatile tools for SMM research, *Coord. Chem. Rev.*, 2015, **289-290**, 238-260.

63. C. Y. Chow, R. Guillot, E. Rivière, J. W. Kampf, T. Mallah and V. L. Pecoraro, Synthesis and magnetic characterization of Fe(III)-based 9-Metallacrown-3 complexes which exhibit magnetorefrigerant properties, *Inorg. Chem.*, 2016, **55**, 10238-10247.

64. M. S. Muravyeva, G. S. Zabrodina, M. A. Samsonov, E. A. Kluev, A. A. Khrapichev, M. A. Katkova and I. V. Mukhina, Water-soluble tetraaqua Ln(III) glycinehydroximate 15-metallacrown-5 complexes towards potential MRI contrast agents for ultra-high magnetic field, *Polyhedron*, 2016, **114**, 165-171.

65. M. A. Katkova, G. S. Zabrodina, M. S. Muravyeva, A. S. Shavyrin, E. V. Baranov, A. A. Khrapichev and S. Y. Ketkov, Facile one-pot route toward water-soluble lanthanide-copper-glycinehydroximate 15-metallacrown-5 complexes, *Eur. J. Inorg. Chem.*, 2015, 5202-5208.

66. T. N. Parac-Vogt, A. Pacco, P. Nockemann, S. Laurent, R. N. Muller, M. Wickleder, G. Meyer, L. Vander Elst and K. Binnemans, Relaxometric study of copper [15] metallacrown-5 gadolinium complexes derived from alpha-aminohydroxamic acids, *Chem. Eur. J.*, 2006, **12**, 204-210.

67. J. Jankolovits, C. M. Andolina, J. W. Kampf, K. N. Raymond and V. L. Pecoraro, Assembly of Near-Infrared Luminescent Lanthanide Host(Host-Guest) Complexes With a Metallacrown Sandwich Motif, *Angew. Chem. Int. Ed.*, 2011, **50**, 9660-9664.

68. G. M. Sheldrick, A short history of *SHELX*, *Acta. Cryst. A*, 2008, **64**, 112-122.

69. A. L. Spek, *Platon, a multipurpose crystallographic tool*, Utrecht University; Utrecht, The Netherlands, 2001.

70. A. Ruiz-Martinez, D. Casanova and S. Alvarez, Polyhedral structures with an odd number of vertices: nine-atom clusters and supramolecular architectures, *Dalton Trans.*, 2008, 2583-2591.

71. S. Tobita, M. Arakawa and I. Tanaka, The paramagnetic metal effect on the ligand localized S1-to-T1 intersystem crossing in rare earth metal complexes with methyl salicylate, *J. Phys. Chem.*, 1985, **89**, 5649-5654.

72. W. T. Carnall, P. R. Fields and K. Rajnak, Electronic energy levels in the trivalent lanthanide aquo ions II. Gd(III). Absorption Spectra, *J. Chem. Phys.*, 1968, **49**, 4443-4446.

73. M. Ganapathi, S. V. Eliseeva, N. R. Brooks, D. Soccol, J. Fransaer and K. Binnemans, Electrodeposition of luminescent composite metal coatings containing rare-earth phosphor particles, *J. Mater. Chem.*, 2012, **22**, 5514-5522.

74. H. Wei, Z. Zhao, C. Wei, G. Yu, Z. Liu, B. Zhang, J. Bian, Z. Bian and C. Huang, Antiphotobleaching: a type of structurally rigid chromophore ready for constructing highly luminescent and highly photostable europium complexes, *Adv. Funct. Mater.*, 2016, **26**, 2085-2096.

75. A. Beeby, I. M. Clarkson, R. S. Dickins, S. Faulkner, D. Parker, L. Royle, A. S. de Sousa, J. A. G. Williams and M. Woods, Non-radiative deactivation of the excited states of europium, terbium and ytterbium complexes by proximate energy-matched OH, NH and CH oscillators: an improved luminescence method for establishing solution hydration states, *J. Chem. Soc., Perkin Trans. 2*, 1999, 493-503.

76. M. H. V. Werts, R. T. F. Jukes and J. W. Verhoeven, The emission spectrum and the radiative lifetime of Eu^{3+} in luminescent lanthanide complexes, *Phys. Chem. Chem. Phys.*, 2002, **4**, 1542-1548.

77. W. T. Carnall, P. R. Fields and K. Rajnak, Electronic energy levels in the trivalent lanthanide aquo ions IV. Eu(III). Absorption Spectra, *J. Chem. Phys.*, 1968, **49**, 4450-4455.

78. W. T. Carnall, P. R. Fields and K. Rajnak, Electronic energy levels in the trivalent lanthanide aquo ions III. Tb(III). Absorption Spectra, *J. Chem. Phys.*, 1968, **49**, 4447-4449.

79. W. T. Carnall, P. R. Fields and K. Rajnak, Electronic energy levels in the trivalent lanthanide aquo ions I. Pr(III), Nd(III), Pm(III), Sm(III), Dy(III), Ho(III), Er(III) and Tm(III), *J. Chem. Phys.*, 1968, **49**, 4424-4442.

80. J.-C. G. Bünzli and S. V. Eliseeva, in *Lanthanide Luminescence*, eds. P. Hänninen and H. Härmä, Springer Berlin Heidelberg, 2011, vol. 7, ch. 3, pp. 1-45.

81. G. L. Law, T. A. Pham, J. D. Xu and K. N. Raymond, A single sensitizer for the excitation of visible and NIR lanthanide emitters in water with high quantum yields, *Angew. Chem. Int. Ed.*, 2012, **51**, 2371-2374.

82. Z. Ahmed and K. Iftikhar, Sensitization of visible and NIR emitting lanthanide(III) ions in noncentrosymmetric complexes of hexafluoroacetylacetone and unsubstituted monodentate pyrazole, *J. Phys. Chem. A*, 2013, **117**, 11183-11201.

83. N. Wartenberg, O. Raccurt, E. Bourgeat-Lami, D. Imbert and M. Mazzanti, Multicolour optical coding from a series of luminescent lanthanide complexes with a unique antenna, *Chem. Eur. J.*, 2013, **19**, 3477-3482.

84. A. F. Martins, S. V. Eliseeva, H. F. Carvalho, J. M. Teixeira, C. T. Paula, P. Hermann, C. Platas-Iglesias, S. Petoud, E. Toth and C. F. Geraldes, A bis(pyridine N-oxide) analogue of DOTA: relaxometric properties of the Gd(III) complex and efficient sensitization of visible and NIR-emitting lanthanide(III) cations including Pr(III) and Ho(III), *Chem. Eur. J.*, 2014, **20**, 14834-14845.

85. J.-C. G. Bünzli, A.-S. Chauvin, H. K. Kim, E. Deiters and S. V. Eliseeva, Lanthanide luminescence efficiency in eight- and nine-

coordinate complexes: role of the radiative lifetime, *Coord. Chem. Rev.*, 2010, **254**, 2623-2633.
86. C. Doffek and M. Seitz, The radiative lifetime in near-ir-luminescent ytterbium cryptates: the key to extremely high quantum yields, *Angew. Chem. Int. Ed.*, 2015, **54**, 9719-9721.
87. N. M. Shavaleev, S. V. Eliseeva, R. Scopelliti and J.-C. G. Bünzli, Influence of symmetry on the luminescence and radiative lifetime of nine-coordinate europium complexes, *Inorg. Chem.*, 2015, **54**, 9166-9173.
88. N. M. Shavaleev, R. Scopelliti, F. Gumy and J.-C. G. Bünzli, Surprisingly bright near-infrared luminescence and short radiative lifetimes of ytterbium in hetero-binuclear Yb-Na chelates, *Inorg. Chem.*, 2009, **48**, 7937-7946.